

Inelastic deformation behavior of $\text{La}_{0.6}\text{Sr}_{0.4}\text{FeO}_3$ perovskiteNina Orlovskaya^{a)}*Department of Materials Science and Engineering, Michigan Technological University, Minerals and Materials Building, 1400 Townsend Drive, Houghton, Michigan 49931*

Harlan Anderson

*Electronic Materials Applied Research Center, University of Missouri-Rolla, 1870 Milner Circle, Rolla, Missouri 65409*Mykola Brodnikovskyy and Mykola Lugovy^{b)}*Institute for Problems of Materials Science, 3 Krzhizhanovskii Street, Kiev-14203142, Ukraine*

Michael John Reece

Department of Materials, Queen Mary University of London, Mile End Road, London E1 4NS, United Kingdom

(Received 10 December 2005; accepted 6 May 2006; published online 19 July 2006)

Inelastic deformation behavior of the rhombohedral $\text{La}_{0.6}\text{Sr}_{0.4}\text{FeO}_3$ perovskite is reported. Such behavior is very similar to the ferroelastic deformation of LaCoO_3 or lead zirconate titanate perovskites, except that no twin structure was found to exist in $\text{La}_{0.6}\text{Sr}_{0.4}\text{FeO}_3$. The possible mechanisms responsible for such nonlinear deformation behavior are discussed. © 2006 American Institute of Physics. [DOI: [10.1063/1.2218026](https://doi.org/10.1063/1.2218026)]

Ceramics are brittle materials because they cannot deform plastically. During the deformation there is only a small absorption of energy, and a linear stress-strain relationship is observed up to the failure of the material. However, some ceramic materials have a low fracture toughness of $1-3 \text{ MPa m}^{1/2}$, but show a nonelastic deformation behavior.^{1,2} Several mechanisms can be responsible for such inelastic deformation: ferroelastic domain switching,³ phase transformation,³ dislocation/point defect motion,^{2,4} grain rotation,^{5,6} or microcracking.^{7,8}

$\text{La}_{1-x}\text{Sr}_x\text{FeO}_3$ (LSF) perovskite ceramics are important materials for application in solid oxide fuel cells, oxygen separation membranes, sensors, and catalysts. The crystal structure of LSF ceramics at ambient temperature is a function of Sr content. While pure LaFeO_3 has an orthorhombic structure ($Pnma$ space group), it transforms to a rhombohedral structure ($R\bar{3}c$ space group) as the amount of Sr content increases from 0.4 to 0.7. The system becomes cubic when the Sr content is in excess of 0.8.⁹ While there are reports on the mechanical behavior of pure LaFeO_3 perovskites,¹⁰ no mechanical properties have been reported for $\text{La}_{0.6}\text{Sr}_{0.4}\text{FeO}_3$ despite its superior mixed ionic electronic conductivity. However, the reliability and mechanical performance of this material is of great importance in the current development of durable devices for energy systems.

Here we report the discovery of inelastic deformation behavior for $\text{La}_{0.6}\text{Sr}_{0.4}\text{FeO}_3$ during compression testing. Single loading/unloading along with incremental cycling were performed to study the response of polycrystalline LSF perovskite to compressive loading.

The $\text{La}_{0.6}\text{Sr}_{0.4}\text{FeO}_3$ perovskite powders were isostatically pressed at 207 MPa followed by sintering at 1200 °C in air for 24 h.¹¹ Parallelepipeds $\approx 3 \times 3 \times 6 \text{ mm}^3$ were cut and machined from the sintered, 5% porous, samples. To remove the deformed surface layer introduced during machining, some samples were annealed at 1100 °C for 4 h.

Compression tests were performed in a servohydraulic test machine (Instron 8500) with a 20 kN load cell. The compression axis was along the longest dimension of the sample. Samples were compressed in air at room temperature at a constant loading/unloading crosshead speed of 0.01 mm/min. Both monotonic and cyclic loadings were performed. The cyclic compression tests were performed in the following way: loading-unloading (first cycle), loading-unloading to the same load (second cycle), incremental loading and two more cycles (first and second) at the new load, and so on. The displacement/strain was measured using a purpose built capacitance device with an annular active ring, and, therefore, the measured displacement was effectively the average of the displacements in all angular directions around the specimen. The resolution of the device was about 0.1 μm .

X-ray diffraction analysis (XRD) (Siemens diffractometer, $\text{Cu K}\alpha$ radiation) was performed to characterize the phase composition of the perovskites. A JEOL JEM-3010 transmission electron microscope (TEM) with energy dispersive spectroscopy (EDS) analysis was used to characterize the microstructure and the chemical composition of the grains.

The crystal structure of LSF has been studied in detail.¹¹ It was found that the rhombohedral distortion that exists in this perovskite was too small to be identified in XRD, patterns. The same was found in the present study, where no splitting of the peaks could be detected by XRD and, therefore, the structure could only be identified as cubic (space

^{a)} Author to whom correspondence should be addressed; electronic mail: norlovsk@mtu.edu

^{b)} Electronic mail: nil2903@gmail.com

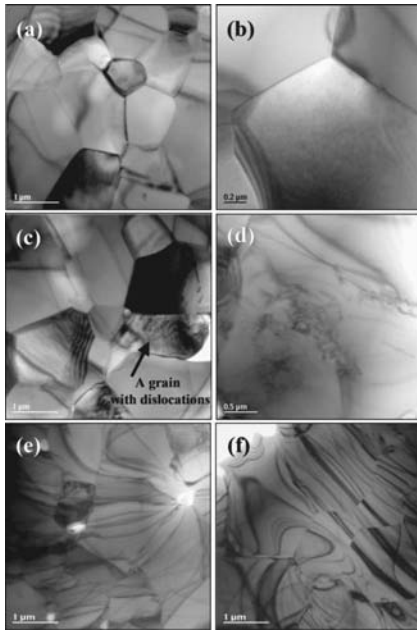


FIG. 1. TEM micrograph showing a grain structure of LSF. [(a) and (b)] Grains are single domains with average grain sizes of 1–3 μm . [(c) and (d)] Grains with dislocations. [(e) and (f)] Grains with bend contours due to local bending of the crystals.

group $Pm\bar{3}m$). However, when neutron diffraction was employed, excellent refinement results were obtained for a structure with a rhombohedral cell (space group $R\bar{3}c$).¹¹

The grain microstructure, with an average grain size of 1–3 μm and some small amount of the porosity of LSF perovskite, is shown in Figs. 1(a)–1(f). The average chemical composition of the grains was found to be La-31.6 at. %, Sr-20.8 at. %, and Fe-47.6 at. %. No domains, twins, antiphase boundaries, stacking faults, or other planar defects were observed. This is perfectly in line with XRD diffraction data where no splitting of the diffraction peaks due to the formation of a twin structure was found. Some grains contain significant numbers of dislocations [Fig. 1(d)] and bend contours [Figs. 1(e) and 1(f)].

A typical loading/unloading curve for LSF is presented in Fig. 2(a), in which certain characteristic stages of deformation can be distinguished. After an initial elastic deformation (region I), the behavior becomes highly nonlinear (region II) due to “easy” deformation. An inflection point occurs at ~ 138 MPa due to a transition from easy deformation to hardening or exhaustion. Upon unloading the perovskite first undergoes an elastic recovery (region III) followed by a nonlinear behavior. The elastic strain, recoverable inelastic (unloading and relaxation) strain, remanent strain, and hysteresis area could be determined from the stress-strain curves (Table I). At zero stress there is some relaxation recovery of the strain. The total recoverable inelastic strain is defined as the sum of the recoverable inelastic strain and the relaxation strain. A remanent strain is induced in the deformed samples. If the ceramics are heat treated the strain can be fully recovered, and a shape memory effect is observed.

A number of researchers explained similar hysteresis and gradual transition from softening to hardening behavior with

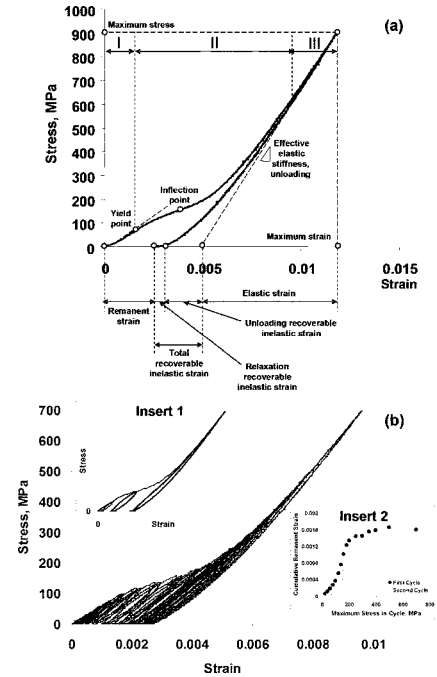


FIG. 2. Compression test of $\text{La}_{0.6}\text{Sr}_{0.4}\text{FeO}_3$ perovskite. (a) I-area of elastic deformation; II-area of inelastic deformation; III-area of elastic deformation at high stress level. Stress-strain diagram of $\text{La}_{0.6}\text{Sr}_{0.4}\text{FeO}_3$ perovskite with cyclic loading. (b) Insert 1-cumulative stress-strain diagram built from the maximum stress points for all cycles showing schematically separate hysteresis loops in different cycles; insert 2-cumulative remanent strain measured from first and second cycles.

increase in applied stress by a domain switching/twinning process. However, both XRD and TEM analyses confirmed that no twins/domains existed in LSF perovskite before loading. Since grains with numerous dislocations have been demonstrated there is a possible contribution from dislocation movement to the observed inelastic behavior. A contribution from microcracking can be ruled out of consideration because the elastic stiffness of the material actually increases with increase of applied load.

Figure 2(b) shows the hysteresis loops generated in LSF with cyclic compression with incremental load. The shape of the hysteresis during cycling closely resembles the shape of the hysteresis produced in the single loading experiment [see Fig. 2(a)]. Insert 1 shows the total hysteresis loop reconstructed using the maximum stress in each single cycle, with three individual loops shown for illustration. Insert 2 of Fig.

TABLE I. Hysteresis parameters of the $\text{La}_{0.6}\text{Sr}_{0.4}\text{FeO}_3$ compression deformation curve during single loading/unloading.

Parameters	Annealed
Maximum stress (MPa)	898
Maximum strain	0.011 8
Elastic modulus under unloading (GPa)	131
Inflection point (MPa)	138
Hysteresis loop area (MPa)	0.571
Elastic strain	0.006 7
Reversible inelastic strain	0.002 4
Relaxation strain	0.000 16
Irreversible strain	0.002 6

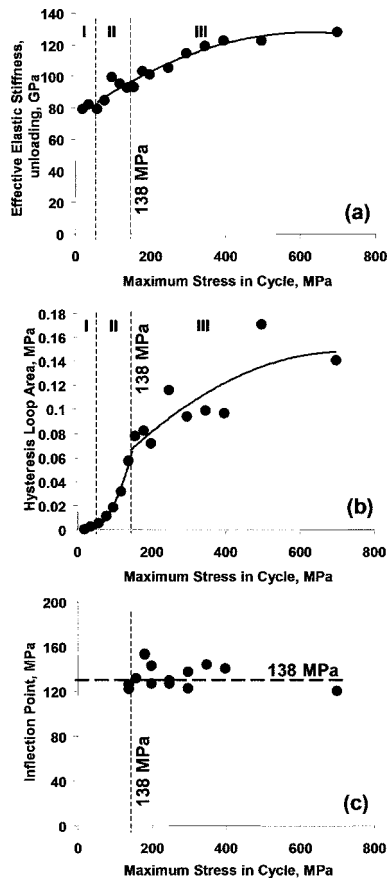


FIG. 3. (a) Effective elastic stiffness, (b) hysteresis loop area, and (c) inflection point vs maximum stress in a cycle. I-zone of elastic deformation; II-zone of inelastic deformation before inflection point; III-zone of inelastic deformation after inflection point.

2(b) shows the evolution of the cumulative remanent strain in the first and second cycles of the incremental loading. As one can see, there are three stages of strain accumulation during cycling: first stage up to 100 MPa of maximum stress in the cycle, second stage between 100 and 200 MPa where the cyclic loading initially produces a significant increment in the cumulative strain, and third stage where the strain eventually saturates and remains almost constant. No more cumulative strain increase occurs for the 500–700 MPa maximum stress cycles. Although the behavior is similar for both the first and the second cycles, the increment of the remanent strain is significantly higher for the first cycle.

The variation of the effective elastic stiffness as a function of applied stress is shown in Fig. 3(a). The effective elastic stiffness was determined as the slope of the tangent of stress-strain curve at the beginning of each unloading. For the first three cycles at low maximum stress level (20, 40, and 60 MPa), no hysteresis was observed and the effective elastic stiffness remained constant (zone I). At higher stresses the effective elastic stiffness increased. This behavior of effective elastic stiffness for inelastically deformed $\text{La}_{0.6}\text{Sr}_{0.4}\text{FeO}_3$ perovskite has not been reported before. It does, however, have important implications in, for instance, the calculation of fracture toughness, since the stiffness is not constant for a given material but changes as a function of applied stress.

The hysteresis loop area as a function of maximum stress in a cycle is shown in Fig. 3(b). No hysteresis is observed in the elastic deformation region (zone I). The hysteresis loop area is a quadratic function of the maximum stress in zone II, with a significant increase up to a maximum applied load of 138 MPa. It shows that the inelastic behavior of the material can possibly be explained by some kind of dislocation motion like kinking nonlinear elastic solids.² Above 138 MPa the hysteresis continues to increase but more slowly. The eventual saturation of the hysteresis loop area could be expected at high stresses (>700 MPa).

Figure 3(c) shows the inflection point stress measured in each cycle versus maximum stress. For the cycles with a maximum stress smaller than 138 MPa no inflection point was observed. For the cycles with a maximum stress above 138 MPa, the inflection point was constant at 138 ± 20 MPa. A similar behavior for the inflection point with incremental loading in LaCoO_3 based perovskites has been reported.¹²

In conclusion, we have found that $\text{La}_{0.6}\text{Sr}_{0.4}\text{FeO}_3$ perovskite deforms inelastically in compression. This behavior is very similar to the ferroelastic deformation of lead zirconate titanate or LaCoO_3 perovskite ceramics, except that no domain/twin structure is found in $\text{La}_{0.6}\text{Sr}_{0.4}\text{FeO}_3$. Therefore, domain switching or twinning does not appear to be responsible for the inelastic deformation of this Sr-doped lanthanum ferrite. Since an increase of effective elastic stiffness was found during the compression tests, a phase transformation cannot be excluded as a mechanism responsible for the nonelastic deformation. Another possible mechanism is dislocation motion like kinking nonlinear elastic solids, since a lot of dislocations were found to exist in the grains. Further research is required to determine the details of mechanism responsible for the inelasticity of $\text{La}_{0.6}\text{Sr}_{0.4}\text{FeO}_3$ perovskite.

The help of Dr. A. Nicholls (RRC, University of Illinois, Chicago) with TEM is greatly appreciated. The financial support of the National Science Foundation through Grant No. DMR-0201770, and that of the NATO Collaborative Linkage Grant No. PST.CLG.979411 and Science for Peace Grant No. 980878 are acknowledged.

¹K. Kleveland, N. Orlovskaya, T. Grande, A.-M. Moe, M.-A. Einarsrud, K. Breder, and G. Gogotsi, *J. Am. Ceram. Soc.* **84**, 2029 (2001).

²M. W. Barsoum, T. Zhen, A. Zhou, S. Basu, and S. R. Kalidindi, *Phys. Rev. B* **71**, 134101-1 (2005).

³M. Selten, G. A. Schneider, V. Knoblauch, and R. M. McMeeking, *Int. J. Solids Struct.* **42**, 3953 (2005).

⁴H. Y. Yasuda, K. Nakano, T. Nakajima, M. Ueda, and Y. Umakoshi, *Acta Mater.* **51**, 5101 (2003).

⁵L. Margulies, G. Winter, and H. F. Poulsen, *Science* **291**, 2392 (2001).

⁶N. Orlovskaya, D. Steinmetz, S. Yarmolenko, D. Pai, J. Sankar, and J. Goodenough, *Phys. Rev. B* **72**, 014122-1-7 (2005).

⁷S. Suresh and J. R. Brockenbrough, *Acta Metall.* **36**, 1455 (1988).

⁸J. R. Brockenbrough and S. Suresh, *J. Mech. Phys. Solids* **35**, 721 (1987).

⁹S. E. Dann, D. B. Currie, M. T. Weller, M. F. Thomas, and A. D. Alrawas, *J. Electrochem. Soc.* **134**, 1718 (1987).

¹⁰A. Fossdal, M.-A. Einarsrud, and T. Grande, *J. Eur. Ceram. Soc.* **25**, 927 (2005).

¹¹J. B. Yang *et al.*, *Phys. Rev. B* **66**, 184415-1-9 (2002).

¹²S. Faaland, T. Grande, M.-A. Einarsrud, P. E. Vullum, and R. Holmestad, *J. Am. Ceram. Soc.* **88**, 726 (2005).